Meso-scale turbulence in living fluids

Henricus H. Wensink[a,b], Jörn Dunkel[c,1], Sebastian Heidenreich[d], Knut Drescher[c,e], Raymond E. Goldstein[c], Hartmut Löwen[a], and Julia M. Yeomans[f]

[a]Institute for Theoretical Physics II: Soft Matter, Heinrich-Heine-Universität Düsseldorf, Universitätsstraße 1, D-40225 Düsseldorf, Germany; [b]Laboratoire de Physique des Solides, Université Paris-Sud 11, Bâtiment 510, 91405 Orsay Cedex, France; [c]DAMTP, Centre for Mathematical Sciences, University of Cambridge, Wilberforce Road, Cambridge CB3 0WA, United Kingdom; [d]Physikalisch-Technische Bundesanstalt, Abbestr. 2-12, 10587 Berlin, Germany; [e]Departments of Molecular Biology and Mechanical and Aerospace Engineering, Princeton University, Princeton, NJ 08544; and [f]Rudolf Peierls Centre for Theoretical Physics, University of Oxford, 1 Keble Road, Oxford OX1 3NP, United Kingdom

Edited by David A. Weitz, Harvard University, Cambridge, MA, and approved July 20, 2012 (received for review February 3, 2012)

Turbulence is ubiquitous, from oceanic currents to small-scale biological and quantum systems. Self-sustained turbulent motion in microbial suspensions presents an intriguing example of collective dynamical behavior among the simplest forms of life and is important for fluid mixing and molecular transport on the microscale. The mathematical characterization of turbulence phenomena in active nonequilibrium fluids proves even more difficult than for conventional liquids or gases. It is not known which features of turbulent phases in living matter are universal or system-specific or which generalizations of the Navier–Stokes equations are able to describe them adequately. Here, we combine experiments, particle simulations, and continuum theory to identify the statistical properties of self-sustained meso-scale turbulence in active systems. To study how dimensionality and boundary conditions affect collective bacterial dynamics, we measured energy spectra and structure functions in dense *Bacillus subtilis* suspensions in quasi-2D and 3D geometries. Our experimental results for the bacterial flow statistics agree well with predictions from a minimal model for self-propelled rods, suggesting that at high concentrations the collective motion of the bacteria is dominated by short-range interactions. To provide a basis for future theoretical studies, we propose a minimal continuum model for incompressible bacterial flow. A detailed numerical analysis of the 2D case shows that this theory can reproduce many of the experimentally observed features of self-sustained active turbulence.

low Reynolds number swimming | velocity increment distributions | scaling

Simple forms of life, like amoebae or bacteria, self-organize into remarkable macroscopic patterns (1, 2), ranging from extended networks (3, 4) to complex vortices (5–10) and swarms (11). These structures often bear a striking resemblance to assemblies of higher organisms [e.g., flocks of birds (12) or schools of fish (13, 14)] and present important biological model systems to study nonequilibrium phases and their transitions (15–17). A particularly interesting manifestation of collective behavior in microbial suspensions is the emergence of meso-scale turbulent motion (7, 8, 18, 19). Driven by the microorganisms' self-propulsion and their mutual interactions, such self-sustained "active turbulence" can have profound effects on nutrient mixing and molecular transport in microbiological systems (2, 20–22). However, in spite of recent progress (19, 23–25), the phenomenology of turbulent bacterial dynamics is scarcely understood and a commonly accepted theoretical description is lacking (2, 16, 26). The latter fact may not be surprising given that a comprehensive mathematical characterization of turbulence in conventional fluids has remained elusive after more than a century of intense research (27).

In view of the various physical and chemical pathways through which bacteria may communicate (1, 11, 28), a basic yet unsolved problem is to identify those interactions that are responsible for the emergence of collective behavior in dense suspensions (2, 29, 30). Answering this question is essential for understanding whether physical mechanisms such as flagellar bundling or hydrodynamic long-range interactions are relevant to collective bacterial motion; it is also crucial for constraining the vast number of theoretical models that have been proposed during the past two decades (2, 16, 19, 31, 32) but have yet to be tested against experiments. An equally important, unresolved issue pertains to the "universality" of turbulent phenomena in active systems and their relation to turbulence in passive fluids (27). In ordinary liquids and gases, such as water or air, turbulent vortices form due to external forcing if the Reynolds number (Re), the ratio of inertial to viscous forces, is very large ($\mathrm{Re} \gg 1$). By contrast, bacteria provide an internal microscopic forcing and operate at $\mathrm{Re} \sim 10^{-5}$ (33). It is therefore unclear how, or to what extent, the characteristics of self-sustained turbulent states in microbial suspensions differ from those of classical turbulence in passive fluids.

Here, we combine numerical simulations, high-speed microscopic imaging and continuum theory to identify generic statistical properties of active turbulent motion in dense bacterial systems, using *Bacillus subtilis* as a model organism. Unlike previous investigations of collective bacterial swimming in 2D free-standing films (8) and 3D bulk suspensions with liquid–gas interfaces (7, 24, 25), we conducted experiments in closed quasi-2D and 3D microfluidic chambers to minimize external influences and to compare the effects of boundary conditions and dimensionality. Our analysis focuses on traditional turbulence measures, such as energy spectra and velocity structure functions (27, 34, 35). These quantities have been widely studied for turbulent high-Re Navier-Stokes flow (27, 36–41), but their characteristics are largely unknown for active fluids. We compare our experimental results with large-scale simulations of a 2D minimal model for self-propelled rods. In the past, similar models (42) have proven useful for identifying generic aspects of flocking and swarming in active systems (43, 44). We find that, although the SPR model neglects details of bacterial cell–cell interactions, it is able to reproduce many features of our experimental data, suggesting that collective bacterial dynamics in dense suspensions is dominated by short-range interactions (30). We complement our experiments and particle-based simulation studies by identifying a minimal continuum model for incompressible active flow that combines elements from the Toner–Tu (15–17) and Swift–Hohenberg (45) theories.

Results

Motivation for the SPR Model. Self-motile bacteria may form meso-scale vortex patterns if their concentration is sufficiently large (7, 8, 18, 19). At very high volume fractions ($\phi \gtrsim 40\%$), steric repulsion and other short-range interactions (e.g., lubrication

Author contributions: H.H.W., J.D., S.H., K.D., R.E.G., H.L., and J.M.Y. designed research; H.H.W., J.D., S.H., and K.D. performed research; H.H.W., J.D., S.H., and K.D. contributed equally to the paper; H.H.W. and J.D. analyzed data; and H.H.W., J.D., S.H., K.D., R.E.G., H.L., and J.M.Y. wrote the paper.

The authors declare no conflict of interest.

This article is a PNAS Direct Submission.

Freely available online through the PNAS open access option.

[1]To whom correspondence should be addressed. E-mail: jd548@cam.ac.uk.

This article contains supporting information online at www.pnas.org/lookup/suppl/doi:10.1073/pnas.1202032109/-/DCSupplemental.

forces, flagellar bundling of neighboring cells) can be expected to govern physical reorientation and alignment, whereas intrinsic Brownian motion effects (30) become less important in this collision-dominated high-density regime (46). Chemotaxis (7, 18) can strongly affect bacterial dynamics in droplets or near liquid–gas interfaces but is less relevant in closed chambers as considered in our experiments. Recent direct measurements of individual *Escherichia coli* flow fields (30) suggest that hydrodynamic far-field interactions are negligible for bacterial reorientation, especially when bacteria swim close to a no-slip surface. Earlier experiments (8, 24, 25) on 2D films and 3D bulk suspensions also show that the average swimming speeds of individual bacteria [typically of the order of 10 μm/s in isolation (8, 30)] can be enhanced up to five times through collective hydrodynamic near-field effects. In the simplest approximation, however, a sufficiently dense bacterial suspension can be viewed as a system of deterministic, self-propelled, rod-like particles with an effective swimming speed V (for *B. subtilis* at $\phi \sim 40\%$ we find $V \sim 30$ to 100 μm/s depending on oxygen concentration and boundary conditions). One of our objectives is to test such a minimal model against experiments in the limit of highly concentrated suspensions and to provide systematic guidance for more accurate future models.

Non-Equilibrium Phase Diagram of the SPR Model. To identify generic requirements for the formation of turbulent phases in active systems, we performed simulations of a minimal 2D SPR model with periodic boundary conditions (see *SI Appendix* for details). In its simplest form, the model assumes that a rod-shaped self-propelled particle moves deterministically in the overdamped low-Re regime with an effective swimming speed V, while interacting with the other particles by steric forces. Mutual repulsion is implemented by discretizing each rod into spherical segments and imposing a repulsive Yukawa force potential $\sim \exp(-r/\lambda)/r$, where r is the distance, between the segments of any two rods (i.e., the decay length $\lambda > 0$ defines the effective diameter of a rod of length ℓ). If two sufficiently long rods perform a pair collision, this short-range interaction results in an effective nematic (apolar) alignment, before the rods become pushed apart by the repulsive force.

Depending on the effective volume filling fraction ϕ and the rod aspect ratio a, both defined in terms of the scale parameter λ and rod length ℓ, the SPR model exhibits a range of qualitatively different dynamical phases (Fig. 1). The numerically estimated nonequilibrium phase diagram (Fig. 1*A*) illustrates the importance of the effective particle "shape" in 2D: Upon increasing ϕ, short rods undergo a transition from a dilute state (D), with little or no cooperative motion, to a jammed state (J); this transition can be identified by the mean square displacement per particle, which drops off nearly two orders in magnitude along the transition curve. By contrast, very long rods ($a > 13$) do not jam at moderate filling fractions but exhibit swarming (S) behavior and large spatiotemporal density fluctuations. Generally, the transitions from the dilute phase (D) to cooperative motion (regions S, B and T) can be characterized by the Onsager overlap density (47). Upon increasing ϕ further, very long rods tend to assemble in homogeneous lanes (L), corresponding to quasi-smectic regions of local polar order; the swarming-to-laning transition is signaled by a discontinuous increase in the correlation length of the two-particle velocity correlation function. The swarming (S) and laning (L) phases adjoin a so-called active bionematic (18) phase (B), where vortices and extended jet-like structures coexist (28, 45); this phase is characterized by large fluctuations of the local vortex density. Most importantly for the present study, however, the SPR model predicts homogeneous turbulent states (T) at high filling fractions and intermediate aspect ratios $3 \lesssim a \lesssim 13$, a range that covers typical bacterial values (e.g., $2 \lesssim a \lesssim 4$ for *E. coli* and $2 \lesssim a \lesssim 10$ for *B. subtilis* (*SI Appendix*, Fig. S7). The transition between bionematic and turbulent phase is also signaled by the velocity distribution, correlation functions and density fluctuations (*SI Appendix*, Figs. S3 and S4).

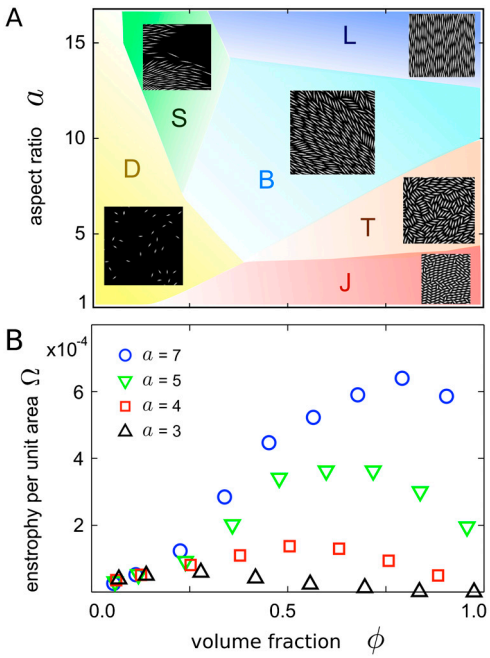

Fig. 1. (*A*) Schematic non-equilibrium phase diagram of the 2D SPR model and snapshots of six distinct phases from simulations: D-dilute state, J-jamming, S-swarming, B-bionematic phase, T-turbulence, L-laning (see also *SI Appendix*, Fig. S2 and Movies S1–S6). Our analysis focuses on the turbulent regime T. (*B*) Enstrophy per unit area Ω in units $(V/\lambda)^2$ for different aspect ratios $a = \ell/\lambda$, obtained from SPR simulations with $N \sim 10^4$ to 10^5 particles. The maxima of the enstrophy indicate the optimal filling fraction for active turbulence and mixing at a given value of the aspect ratio a. Note that values $\phi > 1$ are possible due to the softness of the repulsive force (see *SI Appendix* for simulation parameters).

Homogeneous Turbulent Phase in the SPR Model. A typical turbulent flow state as found in the simulations, and the associated (pseudo-scalar) 2D vorticity field $\omega = \partial_x v_y - \partial_y v_x$, are shown in Fig. 2. The mean local flow field $\boldsymbol{v}(t, \boldsymbol{r})$ at time t and position $\boldsymbol{r}$ was constructed by binning and averaging individual particle velocities, using a spatial resolution similar to that in our experiments (*SI Appendix*). To characterize the emergence of homogeneous turbulence in the SPR model in terms of particle geometry a and effective volume fraction ϕ, we quantify the vortical energy through the enstrophy (27, 34, 35) per unit area, $\Omega = \frac{1}{2}\overline{\langle|\omega(t,\boldsymbol{r})|^2\rangle}$, where brackets $\langle\cdot\rangle$ indicate spatial averages and overbars denote time averages. For slender rods ($a \geq 3$) the mean enstrophy Ω exhibits a maximum when plotted versus the volume fraction ϕ (Fig. 1*B*). This maximum coincides approximately with the transition from the bionematic to the turbulent phase; in a bacterial suspension, it corresponds to the optimal concentration for fluid mixing. Typical aspect ratios of bacterial cell bodies in our experiments lie in the range $2 \lesssim a \lesssim 10$ (mean 6.3 ± 1.2; see *SI Appendix*, Fig. S7). Hence, homogeneous bacterial turbulence should be observable in 2D for a broad range of filling fractions.

Experiments. We test the T-phase of the SPR model against experimental observations of *B. subtilis* at high filling fractions ($\phi \gtrsim 50\%$, see *Materials and Methods*). In contrast to recent investigations of bacterial dynamics in 2D free-standing films (8), on 2D surfaces (44, 48, 49) , and open 3D bulk suspensions (7, 18, 24, 25), bacteria were confined in closed microfluidic chambers to

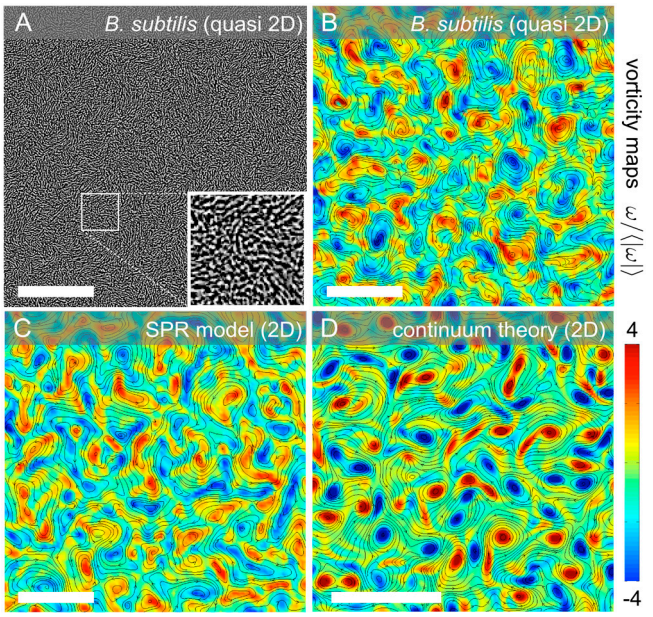

Fig. 2. Experimental snapshot (*A*) of a highly concentrated, homogeneous quasi-2D bacterial suspension (see also Movie S7 and *SI Appendix*, Fig. S8). Flow streamlines $\boldsymbol{v}(t, \boldsymbol{r})$ and vorticity fields $\omega(t, \boldsymbol{r})$ in the turbulent regime, as obtained from (*B*) quasi-2D bacteria experiments, (*C*) simulations of the deterministic SPR model ($a = 5$, $\phi = 0.84$), and (*D*) continuum theory. The range of the simulation data in *D* was adapted to the experimental field of view (217 μm × 217 μm) by matching the typical vortex size. (Scale bars, 50 μm.) Simulation parameters are summarized in *SI Appendix*.

minimize oxygen gradients that may cause anisotropic streaming of the oxytactic *B. subtilis* bacteria (2). To study the effects of dimensionality and boundary conditions, experiments were performed with two different setups: quasi-2D microfluidic chambers with a vertical height H less or equal to the individual body length of *B. subtilis* (approximately 5 μm) and 3D chambers with $H \approx 80$ μm (*SI Appendix*, Figs. S6 and S8 and Movies S7–S10). To focus on the collective dynamics of the microorganisms rather than the solvent flow (24, 50), we determined the mean local motion of *B. subtilis* directly using particle imaging velocimetry (PIV; see also *SI Appendix*). A typical snapshot from a quasi-2D experiment is shown in Fig. 2*A*. As evident from the inset, local density fluctuations that are important in the swarming/flocking regime (48, 49, 51) become suppressed at very high filling fractions (*SI Appendix*, Fig. S5). The corresponding flow fields (Fig. 2*B* and *SI Appendix*, Fig. S8) were used for the statistical analysis presented below.

Continuum Theory. The analytical understanding of turbulence phenomena hinges on the availability of simple yet sufficiently accurate continuum models (27). Considerable efforts have been made to construct effective field theories for active systems (15–17, 19, 31, 32, 52–54), but most of them have yet to be tested quantitatively against experiments. Many continuum models distinguish solvent velocity, bacterial velocity and/or orientational order parameter fields, resulting in a prohibitively large number of phenomenological parameters and making comparison with experiments very difficult. Aiming to identify a minimal hydrodynamic model of self-sustained meso-scale turbulence, we study a simplified continuum theory for incompressible active fluids, by focusing solely on the experimentally accessible velocity field $\boldsymbol{v}(t, \boldsymbol{r})$. By construction, the theory will not be applicable to regimes where density fluctuations are large (e.g., swarming or flocking), but it can provide a useful basis for quantitative comparisons with particle simulations and experiments at high concentrations.

We next summarize the model equations; a detailed motivation is given in *SI Appendix*. Because our experiments suggest that density fluctuations are negligible (Fig. 2*A*) we postulate incompressibility, $\nabla \cdot \boldsymbol{v} = 0$. The dynamics of $\boldsymbol{v}$ is governed by an incompressible Toner–Tu equation (15–17), supplemented with a Swift–Hohenberg-type fourth-order term (45),

$$(\partial_t + \lambda_0 \boldsymbol{v} \cdot \nabla)\boldsymbol{v} = -\nabla p + \lambda_1 \nabla \boldsymbol{v}^2 - (\alpha + \beta|\boldsymbol{v}|^2)\boldsymbol{v} + \Gamma_0 \nabla^2 \boldsymbol{v} - \Gamma_2 (\nabla^2)^2 \boldsymbol{v}, \qquad [1]$$

where p denotes pressure, and general hydrodynamic considerations (52) suggest that $\lambda_0 > 1, \lambda_1 > 0$ for pusher-swimmers like *B. subtilis* (see *SI Appendix*). The (α, β)-terms in Eq. **1** correspond to a quartic Landau-type velocity potential (15–17). For $\alpha > 0$ and $\beta > 0$, the fluid is damped to a globally disordered state with $\boldsymbol{v} = 0$, whereas for $\alpha < 0$ a global polar ordering is induced. However, such global polar ordering is not observed in suspensions of swimming bacteria, suggesting that other instability mechanisms prevail (53). A detailed stability analysis (*SI Appendix*) of Eq. **1** implies that the Swift–Hohenberg-type (Γ_0, Γ_2)-terms provide the simplest generic description of self-sustained meso-scale turbulence in incompressible active flow: For $\Gamma_0 < 0$ and $\Gamma_2 > 0$, the model exhibits a range of unstable modes, resulting in turbulent states as shown in Fig. 2*D*. Intuitively, the (Γ_0, Γ_2)-terms describe intermediate-range interactions, and their role in Fourier space is similar to that of the Landau potential in velocity space (*SI Appendix*). We therefore expect that Eq. **1** describes a wide class of quasi-incompressible active fluids. To compare the continuum model with experiments and SPR simulations, we next study traditional turbulence measures.

Velocity Structure Functions. Building on Kolmogorov's seminal work (55), a large part of the classical turbulence literature (27, 34, 36–38, 40, 41) focuses on identifying the distribution of the flow velocity increments $\delta\boldsymbol{v}(t, \boldsymbol{r}, \boldsymbol{R}) = \boldsymbol{v}(t, \boldsymbol{r} + \boldsymbol{R}) - \boldsymbol{v}(t, \boldsymbol{r})$. Their statistics is commonly characterized in terms of the longitudinal and transverse projections, $\delta v_\parallel = \hat{\boldsymbol{R}} \cdot \delta\boldsymbol{v}$ and $\delta v_\perp = \hat{\boldsymbol{T}} \cdot \delta\boldsymbol{v}$, where $\hat{\boldsymbol{T}} = (\epsilon_{ij}\hat{R}_j)$ denotes a unit vector perpendicular to the unit shift vector $\hat{\boldsymbol{R}} = \boldsymbol{R}/|\boldsymbol{R}|$. The separation-dependent statistical moments of $\delta v_\parallel$ and $\delta v_\perp$ define the longitudinal and transverse velocity structure functions

$$S^n_{\parallel,\perp}(\boldsymbol{R}) := \langle(\delta v_{\parallel,\perp})^n\rangle, \qquad n = 1, 2, \ldots. \qquad [2]$$

These functions have been intensely studied in turbulent high-Re fluids (27, 34, 35, 41) but are unknown for active flow. For isotropic steady-state turbulence, spatial averages $\langle\cdot\rangle$ as in Eq. **2** become time-independent, and the moments $S^n_{\parallel,\perp}$ reduce to functions of the distance $R = |\boldsymbol{R}|$.

Velocity distributions, increment distributions, and structure functions for our numerical and experimental data are summarized in Fig. 3. For the SPR model, the velocity statistics can be calculated either from the raw particle data or from pre-binned flow field data. The two methods produce similar results, and Fig. 3 shows averages based on individual particle velocities. Generally, we find that both the 2D SPR model and the 2D continuum simulations are capable of reproducing the experimentally measured quasi-2D flow histograms (Fig. 3 *A* and *B*) and structure functions (Fig. 3*C*). The maxima of the even transverse structure $S^{2n}_\perp$ signal a typical vortex size R_v, which is substantially larger in 3D bulk flow than in quasi-2D bacterial flow. Unlike their counterparts in high-Re Navier–Stokes flow (27, 34), the structure functions of active turbulence exhibit only a small region of power law growth for $\ell \lesssim R \ll R_v$ and flatten at larger distances (Fig. 3*C*).

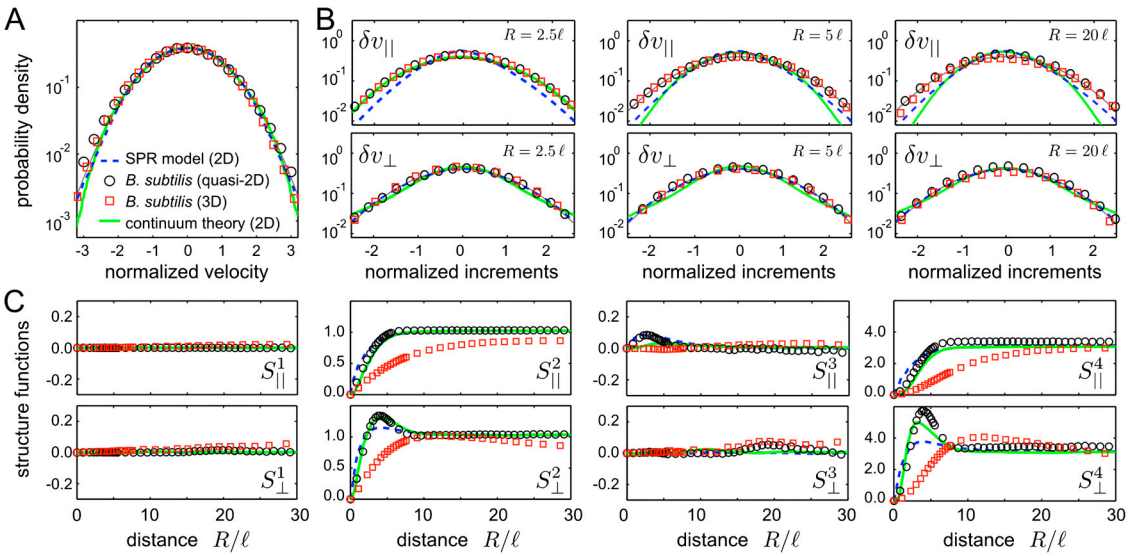

Fig. 3. Velocity statistics of self-sustained turbulent phases in active suspensions. (*A*) The marginal distributions of the normalized Cartesian velocity components $[v_i - \langle v_i\rangle]/[\langle v_i^2\rangle - \langle v_i\rangle^2]^{1/2}_{i=x,y}$ are approximately Gaussian (thin gray line) for experiments, SPR model, and continuum theory. (*B*) The distributions of the longitudinal and transverse velocity increments $\delta v_{\parallel,\perp}$, normalized by their first and second moments $S^{1,2}_{\parallel,\perp}$ are shown for three different separations R. (*C*) Longitudinal and transverse velocity structure functions $S^n_{\parallel,\perp}$ normalized by $\langle v^2\rangle^{n/2}$. The maxima of the even transverse structure functions $S^{2k}_{\perp}$ reflect the typical vortex size R_v , which is significantly larger in the 3D experiments. Experimental and theoretical data points are spatio-temporal averages over two orthogonal directions in *A* and *B* and all directions in *C*, yielding a typical sample size $>10^6$ per plotted data point in *C*. Histograms and structure functions for quasi-2D (3D) curves were obtained by combining PIV data from two (15) movies, respectively, representing an average over $2 \times 1{,}000$ (15×300) frames. Simulation parameters are identical to those in Fig. 2 and summarized in *SI Appendix*. Error bars are smaller than symbols.

Velocity Correlations and Flow Spectra. The energy spectrum $E(k)$, formally defined by $\langle \boldsymbol{v}^2\rangle = 2\int_0^\infty E(k)dk$, reflects the accumulation of kinetic energy over different length scales. By virtue of the Wiener–Khinchine theorem (27), $E(k)$ can be estimated by Fourier transformation of the equal-time two-point velocity correlation function, yielding in d dimensions

$$E_d(k) = \frac{k^{d-1}}{C_d}\int d^dR\, \mathrm{e}^{-i\boldsymbol{k}.\boldsymbol{R}}\langle \boldsymbol{v}(t,\boldsymbol{r})\cdot\boldsymbol{v}(t,\boldsymbol{r}+\boldsymbol{R})\rangle, \qquad [3]$$

where $C_2 = 2\pi$ and $C_3 = 4\pi$. Normalized velocity correlation functions $\langle \boldsymbol{v}(t,\boldsymbol{r})\cdot\boldsymbol{v}(t,\boldsymbol{r}+\boldsymbol{R})\rangle$ and spectra $E_d(k)$ for our data are summarized in Fig. 4. The crossover from positive to negative correlations indicates again the typical vortex size R_v, in agreement with Fig. 3*C* and previous findings for open 3D bulk systems (7, 18).

In bacterial suspensions, the microorganisms inject kinetic energy on small scales $R \sim \ell$, setting the upper bound $k_\ell = 2\pi/\ell$ for the spectral range of the bacterial fluid. For both experiments and simulations, we observe turbulent vortices on scales $R > \ell$, which formally correspond to the energy-inertial range $k < k_\ell$ in classical 2D turbulence (34, 35). Our experimental and numerical data suggest asymptotic power law scaling regimes for small and large k-values (see Fig. 4*B*), but the power-law exponents differ from the characteristic $k^{-5/3}$-decay of 2D Kolmogorov–Kraichnan turbulence (39); see discussion below. The spectra for the 2D continuum model and the quasi-2D bacteria experiments are in good agreement, both showing large-k scaling with approximately $E(k) \sim k^{-8/3}$ and small-k scaling with roughly $E(k) \sim k^{+5/3}$. The asymptotic spectra for the 2D SPR model and the 3D experimental data look qualitatively similar but do also exhibit an intermediate plateau region, which indicates that kinetic energy is more evenly distributed over a range of scales.

Conclusions

SPR Model vs. Experiment. The deterministic SPR model provides a simplified description of the bacterial dynamics, because it neglects not only elastic properties of flagella and cell body but also hydrodynamic interactions and orientational fluctuations due to intrinsic swimming variability and thermal effects (30, 46). Notwithstanding, at high concentrations, such a minimal model reproduces remarkably well the flow velocity distributions and the structure functions from our quasi-2D *B. subtilis* experiments and the 2D continuum simulations (Fig. 3). This implies that hydrodynamic interactions per se are not required for the formation of self-sustained turbulence in dense suspensions—self-propulsion, a rod-like shape and volume exclusion interactions are sufficient (this raises the question whether the optimization of collective behavior may have been a factor in the evolution of bacterial shapes). However, to achieve a better quantitative agreement, particle-based future studies should focus on more realistic models that account for hydrodynamic near-field interactions and intrinsic randomness in bacterial swimming (30). The

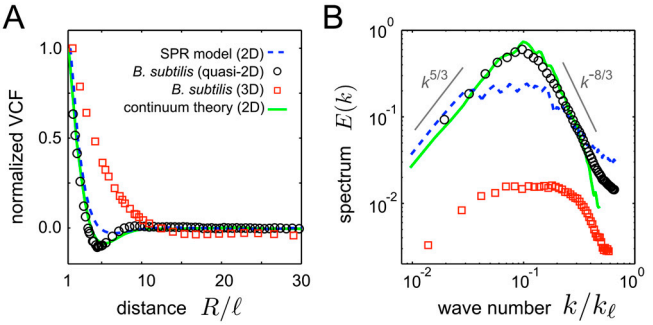

Fig. 4. Equal-time velocity correlation functions (VCFs), normalized to unity at $R = \ell$, and flow spectra for the 2D SPR model ($a = 5$, $\phi = 0.84$), *B. subtilis* experiments, and 2D continuum theory based on the same data as in Fig. 3. (*A*) The minima of the VCFs reflect the characteristic vortex size R_v (48). Data points present averages over all directions and time steps to maximize sample size. (*B*) For bulk turbulence (red squares) the 3D spectrum $E_3(k)$ is plotted ($k_\ell = 2\pi/\ell$), the other curves show 2D spectra $E_2(k)$. Spectra for the 2D continuum theory and quasi-2D experimental data are in good agreement; those of the 2D SPR model and the 3D bacterial data show similar asymptotic scaling but exhibit an intermediate plateau region (spectra multiplied by constants for better visibility and comparison).

experimental results presented above provide a benchmark for evaluating such microscopic models (56).

Continuum Model and "Universality". The good agreement of the structure functions, spatial and temporal flow correlations (see also *SI Appendix*, Fig. S9), and spectra from the 2D continuum theory with those from the quasi-2D experiments suggests that this theory could be a viable model for dense suspensions. Because the instability mechanism in the continuum theory arises from a generic small-wave number expansion in Fourier space (see *SI Appendix*) that is analogous to the Landau expansion in order-parameter space for second-order phase transitions, we expect that the model applies to a wide range of quasi-incompressible active fluids. This would imply that meso-scale turbulent structures in these systems share "universal" long-wave length characteristics. We note that the theory as formulated in Eq. **1** only accounts for leading terms up to fourth-order and, therefore, becomes inaccurate for large velocities and wave numbers (see tails in Figs. 3 *A* and *B* and 4*B*). Nevertheless, this continuum model appears to capture the main statistical and dynamical features of the experimental data. Important future challenges include the analytical prediction of active flow spectra from Eq. **1**, detailed numerical studies of 3D bacterial bulk flows and comparisons of our experimental and numerical data with $\boldsymbol{Q}$-tensor models and other multi-order parameter theories (2, 16, 19, 31, 32).

Dimensionality, Boundaries, and Hydrodynamic Interactions. The quasi-2D experiments allow us to compare with 2D simulations that come close to experimental system sizes. Freestanding thin films (8) and bacterial mono-layers on open surfaces (44, 49), which may be more prone to intrinsic instabilities and external fluctuations, provide an alternative but nonequivalent realization of a 2D bacterial fluid. The crucial difference between freestanding 2D films and our closed quasi-2D setup is that the presence of no-slip boundaries in our experiments suppresses hydrodynamic long-range interactions between bacteria due to cancellation effects from the hydrodynamic images: An isolated dipole-like swimmer [as *E. coli* (30) and, most likely, *B. subtilis*] creates a stroke-averaged far-field flow that decays as approximately $1/r^2$ with distance r in a 3D fluid. When the same swimmer moves parallel to a nearby solid surface in an otherwise semi-infinite fluid, the flow components parallel to the boundary decay faster approximately $1/r^4$ (30). If, however, the swimmer is closely confined between two parallel no-slip walls, as in our quasi-2D experiments with $H \sim 4$ μm, then the flow field becomes exponentially damped at distances $|r| \gg H$ (57). By contrast, in freestanding 2D films the flow field generated by an isolated microorganism has a much longer range approximately $1/r$ (22, 58), suggesting that hydrodynamic interactions could play a more important role for collective behavior in these systems (8). The fact that the typical vortex size in 3D is larger than in quasi-2D could indicate stronger short-to-intermediate-distance hydrodynamic coupling in 3D bulk flow; it would therefore be interesting to perform a similar analysis for thin-film data (8). Generally, however, we expect hydrodynamic far-field interactions to be less important for the dynamics in very dense suspensions due to mutual hydrodynamic screening (59) and the small magnitude of bacterial flows fields (30), but they could act as a destabilizing noise (54, 60).

Low-Re vs. High-Re Turbulence. Conventional high-Re turbulence arises from energy input on large scales (e.g., stirring or shearing). In 3D flow the injected energy is redistributed to smaller scales via an energy-inertial downward cascade with $E_3 \sim k^{-5/3}$ (27). In 2D films, due to the suppression of vortex stretching (34, 35), there can be both an energy-inertial upward cascade with $E_2 \sim k^{-5/3}$ and an enstrophy-transfer downward cascade with $E_2 \sim k^{-3}$ (39). Remarkably, viscoelastic polymer solutions can exhibit turbulent features (e.g., spectral power law scaling) at Reynolds numbers as low as 10^{-3}, facilitated by a slow nonlinear response to external shear due to long intrinsic relaxation times of the polymers (61, 62). Our simulations and experiments suggest asymptotic spectral power law decays toward the bacterial energy injection scale $k_\ell = 2\pi/\ell$ that resemble the energy-inertial regime of classical turbulence but, due to viscous damping by the low-Re solvent, extend over a smaller range of length scales (roughly up to 10ℓ). The latter fact is reminiscent of viscoelastic turbulence (61), although the underlying physical mechanisms are very different.

In conclusion, bacterial or, more generally, self-sustained active "turbulence," shares some qualitative characteristics with classical turbulence on small scales while differing on larger scales. Our detailed statistical analysis shows that, as with inertial turbulence, a complete quantitative understanding of turbulent behavior in active systems poses a challenging task. The combined experimental, theoretical, and numerical results presented here may provide both qualitative and quantitative guidance for future studies that aim at identifying the basic principles of dynamical self-organization in living fluids.

Materials and Methods

B. subtilis cells (wild type strain 168) were streaked from a −80 °C stock onto an LB medium plate containing 1.5% agar. The plates were incubated at 37 °C for 12 h. A single colony from the plates was used to inoculate an overnight culture in Terrific Broth (Sigma), which was then back-diluted 1:200 into 50 mL of fresh tryptone broth, and grown at 37 °C on a shaker to mid-log phase. The culture was then concentrated 400 × by centrifugation at 4,000 × *g* for 3 min, and the pellet was resuspended by gentle vortexing, to not shear off the flagella. The concentrated culture was loaded into a polydimethylsiloxane (PDMS) microfluidic device, which was then sealed to reduce background fluid motion. The microfluidic device consisted of cylindrical measurement chambers (radius 100 μm, height 4 μm for quasi-2D measurements, and radius 750 μm, height 80 μm for 3D measurements). The samples were imaged in bright field with a 40 × /NA 1.4 oil immersion objective on a Nikon TI-E microscope. Images were acquired at 40 fps in 2D (camera: Pike, Allied Vision Technologies), and 100 fps and 200 fps in 3D (camera: Phantom v9.1, Vision Research). Compared with measurements in quasi-2D chambers at the same frame rate, the vertical superposition of bacteria leads to a reduced image quality in 3D samples; we therefore recorded the flow in 3D suspensions at a higher frame rate. For the 3D measurements, we imaged at the bottom and in the middle of the chamber, while for the quasi-2D measurements, we imaged in the middle of the chamber. A detailed description of the theoretical models and numerical methods is given in *SI Appendix*. Raw data and additional experimental movies can be downloaded from http://damtp.cam.ac.uk/user/gold/datarequests.html.

ACKNOWLEDGMENTS. The authors are grateful to Gareth Alexander, Thomas Angelini, Igor Aronson, Markus Bär, Howard Berg, Colm Connaughton, Sujoy Ganguly, Siegfried Hess, Vasily Kantsler, John Lister, Peter Lu, Timothy Pedley, Adriana Pesci, and David Weitz for very helpful discussions. S.H. acknowledges financial support from the Deutsche Forschungsgemeinschaft (DFG), Grant HE5995/1-1. This work was also supported by DFG via SFB TR6 (section D3), Engineering and Physical Sciences Research Council, and European Research Council.

1. Copeland MF, Weibel DB (2009) Bacterial swarming: A model system for studying dynamic self-assembly. *Soft Matter* 5:1174–1187.
2. Koch DL, Subramanian G (2011) Collective hydrodynamics of swimming microorganisms: Living fluids. *Annu Rev Fluid Mech* 43:637–659.
3. Tero A, et al. (2010) Rules for biologically inspired adaptive network design. *Science* 327:439–442.
4. Xavier JB, Martinez-Garcia E, Foster KR (2009) Social evolution of spatial patterns in bacterial biofilms: When conflict drives disorder. *Am Nat* 174:1–12.
5. Kessler JO, Wojciechowski M (1997) *Collective Behavior and Dynamics of Swimming Bacteria* (Oxford University Press, Oxford, UK), pp 417–450.
6. Berg HC (1997) Motile behavior of bacteria. *Phys Today* 53:24–29.
7. Dombrowski C, Cisneros L, Chatkaew S, Goldstein RE, Kessler JO (2004) Self-concentration and large-scale coherence in bacterial dynamics. *Phys Rev Lett* 93:098103.
8. Sokolov A, Aranson IS, Kessler JO, Goldstein RE (2007) Concentration dependence of the collective dynamics of swimming bacteria. *Phys Rev Lett* 98:158102.
9. Riedel IH, Kruse K, Howard J (2005) A self-organized vortex array of hydrodynamically entrained sperm cells. *Science* 309:300–303.

10. Tuval I, et al. (2005) Bacterial swimming and oxygen transport near contact lines. *Proc Natl Acad Sci USA* 102:2277–2282.
11. Kearns DB (2010) A field guide to bacterial swarming motility. *Nat Rev Microbiol* 8:634–644.
12. Cavagna A, et al. (2009) Scale-free correlations in starling flocks. *Proc Natl Acad Sci USA* 107:11865–11870.
13. Katz Y, Ioannou CC, Tunstro K, Huepe C, Couzin ID (2011) Inferring the structure and dynamics of interactions in schooling fish. *Proc Natl Acad Sci USA* 108:18720–18725.
14. Sumpter DJT (2006) The principles of collective animal behaviour. *Philos Trans R Soc B* 261:5–22.
15. Toner J, Tu Y, Ramaswamy S (2005) Hydrodynamics and phases of flocks. *Ann Phys* 318:170–244.
16. Ramaswamy S (2010) The mechanics and statistics of active matter. *Annu Rev Condens Matter Phys* 1:323–345.
17. Toner J, Tu Y (1998) Flocks, herds, and schools: A quantitative theory of flocking. *Phys Rev E* 58:4828–4858.
18. Cisneros LH, Cortez R, Dombrowski C, Goldstein RE, Kessler JO (2007) Fluid dynamics of self-propelled micro-organisms, from individuals to concentrated populations. *Exp Fluids* 43:737–753.
19. Wolgemuth CW (2008) Collective swimming and the dynamics of bacterial turbulence. *Biophys J* 95:1564–1574.
20. Guasto JS, Rusconi R, Stocker R (2012) Fluid mechanics of planktonic microorganisms. *Annu Rev Fluid Mech* 44:373–400.
21. Zaid IM, Dunkel J, Yeomans JM (2011) Lévy fluctuations and mixing in dilute suspensions of algae and bacteria. *J R Soc Interface* 8:1314–1331.
22. Kurtuldu H, Guasto JS, Johnson KA, Gollub JP (2011) Enhancement of biomixing by swimming algal cells in two-dimensional films. *Proc Natl Acad Sci USA* 108:10391–10395.
23. Aranson IS, Sokolov A, Kessler JO, Goldstein RE (2007) Model for dynamical coherence in thin films of self-propelled microorganisms. *Phys Rev E* 75:040901.
24. Ishikawa T, et al. (2011) Energy transport in a concentrated suspension of bacteria. *Phys Rev Lett* 107:028102.
25. Cisneros LH, Kessler JO, Ganguly S, Goldstein RE (2011) Dynamics of swimming bacteria: Transition to directional order at high concentration. *Phys Rev E* 83:061907.
26. Czirók A, Vicsek T (2000) Collective behavior of interacting self-propelled particles. *Physica A* 281:17–29.
27. Frisch U (2004) *Turbulence* (Cambridge University Press, Cambridge, UK).
28. Waters CM, Bassler BL (2005) Quorum sensing: Cell-to-cell communication in bacteria. *Annu Rev Cell Dev Biol* 21:319–346.
29. Sokolov A, Aranson IS (2009) Reduction of viscosity in suspension of swimming bacteria. *Phys Rev Lett* 103:148101.
30. Drescher K, Dunkel J, Cisneros LH, Ganguly S, Goldstein RE (2011) Fluid dynamics and noise in bacterial cell-cell and cell-surface scattering. *Proc Natl Acad Sci USA* 108:10940–10945.
31. Baskaran A, Marchetti MC (2009) Statistical mechanics and hydrodynamics of bacterial suspensions. *Proc Natl Acad Sci USA* 106:15567–15572.
32. Baskaran A, Marchetti MC (2008) Hydrodynamics of self-propelled hard rods. *Phys Rev E* 77:011920.
33. Purcell EM (1977) Life at low Reynolds number. *Am J Phys* 45:3–11.
34. Kellay H, Goldburg WI (2002) Two-dimensional turbulence: A review of some recent experiments. *Rep Prog Phys* 65:845–894.
35. Danilov SD, Gurarie D (2000) Quasi-two-dimensional turbulence. *Usp Fiz Nauk* 170:921–968.
36. Gotoh T, Fukuyama D, Nakano T (2002) Velocity field statistics in homogeneous steady turbulence obtained using a high-resolution direct numerical simulation. *Phys Fluids* 14:1065–1081.
37. Noullez A, Wallace G, Lempert W, Miles RB, Frisch U (1997) Transverse velocity increments in turbulent flow using the RELIEF technique. *J Fluid Mech* 339:287–307.
38. Camussi R, Benzi R (1997) Hierarchy of transverse structure functions. *Phys Fluids* 9:257–259.
39. Kraichnan RH, Montogomery D (1980) Two-dimensional turbulence. *Rep Prog Phys* 43:547–619.
40. Lewis GS, Swinney HL (1999) Velocity structure functions, scaling, and transitions in high-Reynolds-number Couette-Taylor flow. *Phys Rev E* 59:5457–5467.
41. Anselmet F, Gagne Y, Hopfinger EJ, Antonia RA (1984) High-order velocity structure functions in turbulent shear flows. *J Fluid Mech* 140:63–89.
42. Ginelli F, Peruani F, Bär M, Chaté H (2010) Large-scale collective properties of self-propelled rods. *Phys Rev Lett* 104:184502.
43. Darnton NC, Turner L, Rojevsky S, Berg HC (2010) Dynamics of bacterial swarming. *Biophys J* 98:2082–2090.
44. Zhang HP, Be'er A, Florin E-L, Swinney HL (2010) Collective motion and density fluctuations in bacterial colonies. *Proc Natl Acad Sci USA* 107:13626–13630.
45. Swift J, Hohenberg PC (1977) Hydrodynamic fluctuations at the convective instability. *Phys Rev A* 15:319–328.
46. Munk T, Höfling F, Frey E, Franosch T (2009) Effective Perrin theory for the anisotropic diffusion of a strongly hindered rod. *Europhys Lett* 85:30003.
47. Onsager L (1949) The effects of shape on the interaction of colloidal particles. *Ann NY Acad Sci* 51:627–659.
48. Zhang HP, Be'er A, Smith RS, Florin E, Swinney HL (2009) Swarming dynamics in bacterial colonies. *Europhys Lett* 87:48011.
49. Chen X, Dong X, Be'er A, Swinney HL, Zhang HP (2012) Scale-invariant correlations in dynamic bacterial clusters. *Phys Rev Lett* 108:148101.
50. Dunkel J, Putz VB, Zaid IM, Yeomans JM (2010) Swimmer-tracer scattering at low Reynolds number. *Soft Matter* 6:4268–4276.
51. Narayan V, Ramaswamy S, Menon N (2007) Long-lived giant number fluctuations in a swarming granular nematic. *Science* 317:105–108.
52. Pedley TJ (2010) Collective behaviour of swimming micro-organisms. *Exp Mech* 50:1293–1301.
53. Ramaswamy S (2002) Hydrodynamic fluctuations and instabilities in ordered suspensions of self-propelled particles. *Phys Rev Lett* 89:058101.
54. Saintillan D, Shelley M (2008) Instabilities, pattern formation and mixing in active suspensions. *Phys Fluids* 20:123304.
55. Kolmogorov AN (1941) The local structure of turbulence in incompressible viscous fluid for very large Reynolds number. *Dokl Akad Nauk SSSR* 30:299–303.
56. Hernandez-Ortiz JP, Underhill PT, Graham MD (2009) Dynamics of confined suspensions of swimming particles. *J Phys Condens Matter* 21:204107.
57. Liron N, Mochon S (1976) Stokes flow for stokeslet betwen to parallel flat plates. *J Eng Math* 10:287–303.
58. Guasto JS, Johnson KA, Gollub JP (2010) Oscillatory flows induced by microorganisms swimming in two dimensions. *Phys Rev Lett* 105:168102.
59. Muthukumar M, Edwards SF (1983) Screening of hydrodynamic interaction in a solution of rodlike macromolecules. *Macromolecules* 16:1475–1478.
60. Ryan SD, Haines BM, Beryland L, Ziebert F, Aranson IS (2011) Viscosity of bacterial suspensions: Hydrodynamic interactions and self-induced noise. *Phys Rev E* 83:050904(R).
61. Groisman A, Steinberg V (2000) Elastic turbulence in a polymer solution. *Nature* 405:53–55.
62. Goddard C, Hess O, Hess S (2010) Low Reynolds number turbulence in nonlinear Maxwell-model fluids. *Phys Rev E* 81:036310.